Nanostructure and Elastic Modulus of Single Trabecula in Bovine Cancellous Bone

Satoshi YAMADA[1], Shigeru TADANO[1,*], Sakurako FUKUDA[2]

[1] Division of Human Mechanical Systems and Design, Faculty of Engineering, Hokkaido University, N13 W8, Kita-ku, Sapporo, Hokkaido 060-8628, Japan

[2] Division of Human Mechanical Systems and Design, Graduate School of Engineering, Hokkaido University, N13 W8, Kita-ku, Sapporo, Hokkaido 060-8628, Japan

***Corresponding author**

Shigeru Tadano, Ph.D., Professor

Affiliation: Division of Human Mechanical Systems and Design, Faculty of Engineering, Hokkaido University

Postal address: N13 W8, Kita-ku, Sapporo, Hokkaido 060-8628, Japan

Tel/Fax: +81(Japan)-11-706-6405

E-mail: tadano@eng.hokudai.ac.jp

Types of article: Original Articles

Word count: 3474 words (from Introduction to Discussion)

Abstract

We aimed to investigate the elastic modulus of trabeculae using tensile tests and assess the effects of nanostructure at the hydroxyapatite (HAp) crystal scale on the elastic modulus. In the experiments, 18 trabeculae that were at least 3 mm in length in the proximal epiphysis of three adult bovine femurs were used. Tensile tests were conducted using a small tensile testing device coupled with microscopy under air-dried condition. The *c*-axis orientation of HAp crystals and the degree of orientation were measured by X-ray diffraction. To observe the deformation behavior of HAp crystals under tensile loading, the same tensile tests were conducted in X-ray diffraction measurements. The mineral content of specimens was evaluated using energy dispersive X-ray spectrometry. The elastic modulus of a single trabecula varied from 4.5 to 23.6 GPa, and the average was 11.5 ± 5.0 GPa. The *c*-axis of HAp crystals was aligned with the trabecular axis and the crystals were lineally deformed under tensile loading. The ratio of the HAp crystal strain to the tissue strain (strain ratio) had a significant correlation with the elastic modulus ($r = 0.79$; $P < 0.001$). However, the mineral content and the degree of orientation did not vary widely and did not correlate with the elastic modulus in this study. It suggests that the strain ratio may represent the nanostructure of

a single trabecula and would determine the elastic modulus as well as mineral content and orientation. (236 words)

Keywords:

Biomechanics, Cancellous bone, Single trabecula, Elastic modulus, Hydroxyapatite, X-ray diffraction

1. Introduction

Mechanical properties such as elastic modulus, yield strain, and strength of the cancellous bone are essential to understand the changes in bone fracture risk with aging and/or osteoporosis and to evaluate the effects of osteoporotic medicines as well as bone volume fraction and bone mineral density. It is well known that the apparent elastic modulus of the cancellous bone is measured within the range of several hundred MPa to several GPa, and it is much lower than that of the cortical bone. The apparent mechanical properties of the cancellous bone and their relation with structural properties such as bone volume fraction, mineralization, architecture of trabecular networks, and shape of trabeculae in the cancellous bone have been investigated using uniaxial mechanical tests and micro-computed tomography (CT) scans with cubic or cylindrical specimens of the cancellous bone (e.g., Halgrin et al., 2012; Topoliński et al., 2011; Lievers et al., 2010; Perilli et al., 2007; Mittra et al., 2005). The mechanical properties of a single trabecula that constitutes trabecular networks and their nanostructure composed of hydroxyapatite (HAp) crystals and collagen fibrils are important factors in determining the mechanical properties of the cancellous bone. However, only a few

studies have performed mechanical tests of a single trabecula because the mechanical tests of such small specimens are challenging, as reviewed by Carretta et al. (2013a) and Lucchinetti et al. (2000). Furthermore, the nanostructural effects on the mechanical properties of a single trabecula have not been investigated and elucidated, although various studies have been conducted on multiscale mechanical characterization in the cortical bone (e.g., Barkaoui et al., 2014; Yamada et al., 2013; Tadano and Giri, 2011; Feng and Jasiuk, 2011; Gibson et al., 2006; Hoc et al., 2006). Therefore, the present study focused on the mechanical properties of a single trabecula and on the nanostructural effects on its properties.

Tensile tests (Carretta et al., 2013b, 2013c; McNamara et al., 2006; Hernandez et al., 2005; Bini et al., 2002; Rho et al., 1993) and bending tests (Carretta et al., 2013b, 2013c; Hambli and Thurner, 2013; Lorenzetti et al., 2011; Szabó et al., 2011; Jungmann et al., 2011; Busse et al., 2009; Choi and Goldstein, 1992) of a single trabecula were conducted and some studies compared with finite element models (Carretta et al., 2013b, 2013c; McNamara et al., 2006; Hambli and Thurner, 2013; Lorenzetti et al., 2011; Jungmann et al., 2011) to investigate the elastic and post-yield

mechanical properties. Nanoindentation tests were also conducted to obtain the elastic modulus and hardness (Tjhia et al., 2011; Smith et al., 2010; Wolfram et al., 2010; Brennan et al., 2009; Rho et al., 1999); however, the measured values did not necessarily correspond to those obtained in the testing of the whole trabecula. Tensile tests have some advantages over bending tests; for instance, mechanical anisotropy and the inhomogeneous shape of specimens do not severely affect the elastic modulus in the loading direction. In this study, we conducted tensile tests of the whole trabecula to measure the elastic modulus of a single trabecula.

HAp crystals have a hexagonal crystal structure. X-ray diffraction (XRD) is a promising tool for characterizing bone nanocomposites (Tadano and Giri, 2011). Using XRD techniques, it has been reported that on diaphyseal cortical bone, the *c*-axis of HAp crystals aligns along the bone axis, and that the degree of orientation is correlated with the elastic modulus in the bone axis (Yamada et al., 2013). Furthermore, many studies (Yamada et al., 2014, 2013, 2011a, 2011b; Yamada and Tadano, 2013, 2010; Giri et al., 2012, 2009; Dong et al., 2011; Stock et al., 2011; Tadano et al., 2008; Almer and Stock, 2007, 2005; Fujisaki and Tadano, 2007; Gupta et al., 2006; Fujisaki et al., 2006)

have attempted to measure the deformation of HAp crystals in the cortical bone using XRD. For instance, Fujisaki and Tadano (2007) presented the relationship between bone tissue strain and HAp crystal strain under tensile loads *in vitro*. In addition, Almer and Stock (2007, 2005) investigated the strain and stress of the mineral phase under compressive loads *in vitro*. However, the orientation and deformation behavior of HAp crystals in a single trabecula have not been elucidated. As reported in a few studies, Rokita et al. (2005) noted the existence of preferential crystal orientation in the trabecular network of human vertebra using synchrotron X-rays. Akhtar et al. (2011, 2008) described the behavior of averaged HAp crystal strains in the cubic specimen of the cancellous bone under uniaxial compression using synchrotron X-rays. To better understand the nanostructure and its effects on the elastic modulus of a single trabecula, we investigated HAp crystal contents, orientation, and deformation behavior in a single trabecula and compared with the previous findings of the cortical bone.

Therefore, the present study aimed to investigate the nanostructural effects on the elastic modulus of a single trabecula, such as the mineral content and the HAp crystal orientation and deformation behavior in a single trabecula using XRD and

energy dispersive X-ray spectrometry (EDS).

2. Materials and methods

2.1 Specimen preparation

In the experiments, 18 trabeculae that were at least 3 mm in length in the proximal epiphysis of three adult bovine femurs (2-year old) were used (Fig. 1). To measure the orientation of the longitudinal direction of a single trabecula (trabecular axis) in the femoral epiphyses, the trabecular networks in the epiphyses were observed using a microfocus X-ray CT instrument (inspeXio SMX-225CT, Shimadzu, Japan) before specimen extraction. The diaphysis of the femurs was scanned using a tube voltage of 160 kV, a tube current of 40 μA, and a voxel size of 0.398 mm/voxel. The centroid point of the perimeter line of the diaphysis in each cross-section was obtained from the CT images by using ImageJ software and the longitudinal direction of the diaphysis, which was defined as the bone axis, was calculated by approximating a straight line through those points, as shown in Fig. 1(c). Following this, the cancellous bone region was scanned at a voxel size of 0.146 mm/voxel. The trabecular orientation

α was calculated as the angle between the trabecular axis and the bone axis, as shown in Fig. 1(a). After the CT scans, the specimens were collected and fixed to thin metal jigs using superglue, as shown in Fig 1(b). Two small ink marks were placed on the surface of the ends of the specimens to serve as gauge points.

2.2 Trabecular morphology measured by μ-CT

To measure the cross-sectional area and the shape of a single trabecula, the specimens fixed to the jigs were scanned using a microfocus X-ray CT instrument (inspeXio SMX-90CT, Shimadzu, Japan) at a high resolution with a tube voltage of 90 kV, tube current of 110 μA, and voxel size of 0.011 mm/voxel. The average cross-sectional area (*A*), circularity (*Cir*), and aspect ratio (*AR*) in each specimen were calculated from the CT images using ImageJ software.

2.3 Elastic modulus measured using tensile test

The tensile tests were conducted using a small tensile testing device, which consisted of a linear stage (ALS-4011-G1M, Chuo Precision Industrial, Japan) with

high resolution (2 μm) and repeatability (0.3 μm) and a load cell (LTS-1KA, Kyowa, Japan) with high repeatability (0.5% or less) and small hysteresis (within 0.5%), and viewed under a microscope (VH-5000, Keyence, Japan), as shown in Fig. 2. The tissue strain was measured from the distance between the gauge points using the microscope at 1 N intervals from 1 to 8 N. The tissue stress was calculated as the applied load divided by the average cross-sectional area A, and the elastic modulus E of a single trabecula was calculated. The tensile tests were conducted three times under the air-dried condition, and the average E was used for each specimen.

2.4 HAp crystal orientation measured by XRD

As shown in Fig. 3(a), the specimen was perpendicularly irradiated for 10 min with characteristic X-rays of Mo-Kα (λ = 0.071 nm) using an X-ray diffractometer (Ultima IV, Rigaku, Japan) with a collimator of 0.5 mm diameter, at a tube voltage of 40 kV and a tube current of 40 mA. The measurements were conducted three times, and the average value was used for each specimen.

The incident X-rays were diffracted in lattice planes of HAp crystals in

accordance with Bragg's equation. The traveling direction and the intensity of the diffracted X-rays depend on the direction and the number of the lattice planes, respectively. The XRD pattern of the specimen was detected using an X-ray imaging plate (IP) (BAS-SR 127 × 127 mm^2, Fujifilm, Japan) and was read using a scanner (R-axis DS3C, Rigaku, Japan). When the *c*-axis of the HAp crystals aligned along a specific direction in the specimen, the XRD pattern of the (002) plane, which was perpendicular to the *c*-axis, appeared as arcs. In the present study, the *c*-axis orientation of HAp crystals was defined as the direction of the highest intensity of diffracted X-rays from the (002) plane and the degree of *c*-axis orientation of the crystals with respect to the trabecular axis was calculated from Eq. (1) using the XRD pattern of the (002) plane (Yamada et al., 2013; Tadano and Giri, 2011).

$$<\cos^2\beta>=\frac{\int_0^{2\pi} I(\beta)\cos^2\beta|\sin\beta|d\beta}{\int_0^{2\pi} I(\beta)|\sin\beta|d\beta} \quad (1)$$

Here, $I(\beta)$ is the intensity of the diffracted X-rays from the (002) plane at the azimuth angle β in the XRD pattern. If every crystal is completely oriented in the trabecular axis,

$\langle \cos^2\beta \rangle$ is equal to 1.

2.5 HAp crystal deformation behavior measured by XRD

To measure the HAp crystal strains under the tensile test, the tensile tests were also conducted during the XRD measurements under the same air-dried condition.

The HAp crystal strain ε^H in the trabecular axis was calculated from the changes of the interplanar spacing d of the (002) plane in the direction, as in Eq. (2), where θ is the half of diffraction angle and the subscript 0 indicates the nonstrained condition.

$$\varepsilon^H = \frac{d - d_0}{d_0} = \frac{\sin\theta_0 - \sin\theta}{\sin\theta} \quad (2)$$

XRD measurements were performed at 1 N intervals from 1 to 8 N using the same tensile testing device attached to the X-ray diffractometer, as shown in Fig. 3(b). The specimens were irradiated with X-rays using a collimator of 1 mm diameter, at tube voltage of 40 kV and a tube current of 40 mA. The XRD profiles were measured using a

scintillation counter with 2θ value between 11.0° and 12.5°, which included the diffraction angle of the (002) plane of HAp crystals. The measurements were conducted three times at each loading condition, and the three XRD profiles were summed as a profile. The diffraction angle 2θ was defined as the angle at the peak position of the profile, and the peak position was determined by applying the full width at two-thirds maximum (FWTTM) method (Yamada et al., 2011a). The applied tissue strain was calculated from the tensile force obtained by the load cell, A measured by CT scan and E measured in the tensile test without XRD. The ratio of the HAp crystal strain to tissue strain (strain ratio), $\varepsilon^H/\varepsilon$, was calculated by linear approximation.

2.6 Mineral content evaluated by EDS

After the abovementioned measurements, the specimens were embedded in epoxy resin for 24 h and cut at the middle section using a low-speed diamond wheel saw (Model 650, South Bay Technology, USA). The transverse cross-section was ground using emery papers (up to #2000) and buffed using a buffing machine (Model 900, South Bay Technology, USA). The cross-section was observed using a

low-vacuum scanning electron microscope (SEM) (JSM-6360LA, JEOL, Japan) at an accelerating voltage of 15 kV in low vacuum (30 Pa) without evaporation coating. To determine the composition of the chemical elements in the specimens, EDS was performed on five points in the cross-section using the EDS detector attached to the SEM system. To evaluate the mineral content of the specimens, the weight content of calcium and phosphorus v_{Ca+P}, which are derived from HAp, in the detectable elements was calculated by averaging the five regions in each specimen.

2.7 Cortical bone specimens

Five cortical bone specimens ($40 \times 2 \times 1$ mm^3) examined in a previous study (Yamada et al., 2013), which were taken from the middiaphysis of a 2-year-old bovine femur, were used. The elastic modulus of the bone axis, $\langle\cos^2\beta\rangle$, and $\varepsilon^H/\varepsilon$ had been measured under air-dried condition. The transverse cross-section was observed and v_{Ca+P} was measured with the same procedure.

3. Results

Table 1 shows the number of samples examined for each experiment after excluding the unavailable data, mean values, and standard deviations of each parameter of the trabeculae.

The trabecular orientation α ranged from 5.3° to 85.1°, and the average was 53.6 ± 24.7°. The trabeculae used in this study were almost randomly oriented in the cancellous bone. The circularity *Cir* and aspect ratio *AR* were 0.825 ± 0.066 and 1.58 ± 0.33, respectively. Therefore, the trabeculae examined in this study had a rod-like shape and not a plate-like shape. Furthermore, there was a statistically positive correlation between α and A ($r = 0.69$; $P < 0.01$).

As shown in Fig. 4, the tensile tests showed a highly linear stress–strain relation. The elastic modulus E of the trabeculae varied from 4.5 to 23.6 GPa, and the average was 11.5 ± 5.0 GPa.

Figure 5 shows a typical XRD pattern of a single trabecula. The angle between the *c*-axis orientation of HAp crystals and the trabecular axis was 4.03 ± 3.10°. The *c*-axis of the HAp crystals aligned with the trabecular axis and did not depend on α, although the axis in the diaphyseal cortical bone was aligned with the bone axis.

Furthermore, as shown in Fig. 6(a), there was no statistical correlation between E and $\langle\cos^2\beta\rangle$. Figure 6(b) shows a typical deformation behavior of HAp crystals in a single trabecula under tensile loading. HAp crystals were linearly deformed with respect to the applied tissue strain (R^2 = 0.75 ± 0.20), although the R^2 value was too small in the specimens with low $\varepsilon^H/\varepsilon$. As shown in Fig. 6(c), there was a significantly positive correlation between E and $\varepsilon^H/\varepsilon$ (r = 0.79; P < 0.001). Furthermore, including the data of cortical bone specimens (Yamada et al., 2013), there was a significant correlation (r = 0.86; P < 0.001). EDS analysis showed that v_{Ca+P} was 55.8 ± 1.5 wt% in a single trabecula and 62.0 ± 1.2 wt% in the cortical bone. The v_{Ca+P} had positive correlations with A (r = 0.75; P < 0.001) and α (r = 0.49; P < 0.05) in the trabeculae. However, as shown in Fig. 6(d), there was no statistical correlation between E and v_{Ca+P}.

4. Discussion

We measured the elastic modulus of trabeculae in the longitudinal direction taken from the cancellous bone of bovine proximal femurs and investigated the relationship with the nanostructural effects such as mineral content and HAp crystal

orientation and deformation behavior.

The possible sources of errors in this tensile test were sample fixation and alignment, loading pattern and speed, and resolution of CT images. The standard deviation of elastic modulus in the three measurements of each specimen was 1.2 ± 1.2 GPa and R^2 value of the stress–strain relations was 0.98 ± 0.02, suggesting sufficiently high repeatability and linearity of the stress–strain relations. Tensile tests have some advantages over bending tests; however, as Lucchinetti et al. (2000) pointed out, tensile tests of a single trabecula have two main sources of errors: effects of sample fixation and alignment. The deformation of the load cell and the superglue used to fix the specimens onto the jigs during the tests should be considered in the analysis and interpretation of the results. Hence, in the present study, two small ink marks were placed on the surface of the ends of the specimens to serve as gauge points, and the changes in gauge length were measured by microscopy as the specimen underwent displacement. In addition, the specimens were carefully fixed and set on the jigs in terms of sample alignment. Furthermore, we applied tensile loads to the specimens in the stages at a loading speed of 0.2 N/s. Szabó et al. (2011) reported that there was no

correlation between the elastic modulus and strain speed in the three-point-bending tests of trabeculae, suggesting that the loading conditions in the present study might not have had any effect on the elastic modulus. The resolution of CT images may also affect the average cross-sectional area of the specimens and the values of elastic modulus.

In the literature, the elastic modulus of a single trabecula varied in the range of 2–16 GPa under a dry condition (Carretta et al., 2013b, 2013c; Busse et al., 2009; Bini et al., 2002; Rho et al., 1993) and in the range of 1–17 GPa under a wet condition (Lorenzetti et al., 2011; Szabó et al., 2011; Jungmann et al., 2011; McNamara et al., 2006), including different species, ages, locations, size, and mechanical tests. In particular, Carretta et al., (2013c), using tensile tests, indicated that the elastic modulus of dried trabeculae of bovine femurs was 11.8 GPa, and Szabó et al. (2011), using bending tests, indicated that the elastic modulus of wet specimens of bovine femurs varied from 1.1 to 16.5 GPa. These results correspond to those of the present study. One of the limitations of this study was the use of air-dried specimens. The drying process was the same for all the specimens, and the strong correlations may not have been affected in the study. Furthermore, the results of the study were compared with those of

the cortical bone specimens examined in a previous study (Yamada et al., 2013) using almost the same procedure.

In this study, there was no statistical correlation between mineral content and elastic modulus of a single trabecula. However, mineral content was significantly smaller than that of the cortical bone specimens as well as the elastic modulus. Furthermore, $\langle \cos^2\beta \rangle$ had no correlation with the elastic modulus of a single trabecula and was significantly smaller than that of the cortical bone specimens, although there was a significant correlation between them in the cortical bone specimens. This suggests that mineral content and orientation holistically decrease the elastic modulus of the trabecular tissue in comparison with that of the cortical bone; however, the variation of the elastic modulus in a single trabecula could not be sufficiently explained by these factors. The maturation of bone minerals such as chemical impurities and crystallinity will also affect the mechanical properties; however, the variation in the full width at half maximum (FWHM) of the (002) plane peak in XRD profiles was small (1.6%) in the used trabeculae. The effects of maturation of bone mineral are expected to be almost the same in this study.

This study indicated the linear deformation of HAp crystals in a single trabecula with respect to the applied tissue strain under tensile loading and the significant correlation between strain ratio and elastic modulus. Gupta et al. (2006) investigated the strains of HAp crystals and collagen fibrils using synchrotron X-rays and discussed the nanocomposite model of the cortical bone tissue. Hambli and Barkaoui (2012) developed a finite element model of a single mineralized collagen microfibril and discussed the effects of the nanostructure on the mechanical behavior. The strain ratio would represent the nanostructure formed by HAp crystals, collagen fibrils, extrafibrillar matrix, and intermolecular cross-links and would determine the elastic modulus of a single trabecula as well as mineral content and orientation. In the present study, the strain ratio was measured under tensile loading. The deformation behavior in the nanocomposites and the effects of crystal orientation might be affected by tensile/compressive loading. The effects of loading pattern on the properties should also be examined further. The investigation of the deformation behavior of collagen fibrils and extrafibrillar matrix in a single trabecula may be an essential topic to consider in future studies for further elucidating the nanocomposite model of a single

trabecula.

We examined 18 relatively long trabeculae taken from three bovine femurs of the same age and the cancellous bone from where the specimens were extracted had a lower bone volume fraction. In the present study, the mineral content and HAp crystal orientation did not vary widely and did not correlate with the elastic modulus in the trabeculae. The results may relate to the limitations, while the effects of strain ratio on elastic modulus could be observed. Furthermore, the mineral content had a positive correlation with cross-sectional area and trabecular orientation. This suggests that the mineralization may increase with the growth of a single trabecula by reflecting *in vivo* mechanical environments; however, these parameters had no correlation with the elastic modulus. This might also relate to the limitations. To investigate the effects of trabecular size, shape, and region of extraction in the cancellous bone on the nanostructure and the resulting mechanical properties of a single trabecula should be examined to better understand the contributions of the nanostructure to the mechanical properties of a single trabecula and the cancellous bone.

Acknowledgements

This study was supported by JSPS Grant-in-Aid for Scientific Research (A) Grant Number 24240068. The energy dispersive X-ray spectrometry was performed using a low-vacuum scanning electron microscope (JSM-6360LA) at the OPEN FACILITY, Hokkaido University Sousei Hall.

Conflict of Interest Statement

No actual or potential conflicts of interest exist.

References

Akhtar, R., Daymond, M.R., Almer, J.D., Mummery, P.M., 2008. Elastic strains in antler trabecular bone determined by synchrotron X-ray diffraction. Acta Biomaterialia 4, 1677-1687.

Akhtar, R., Daymond, M.R., Almer, J.D., Mummery, P.M., 2011. Lattice strains and load partitioning in bovine trabecular bone. Acta Biomaterialia 7, 716-723.

Almer, J.D., Stock, S.R., 2005. Internal strains and stresses measured in cortical bone via high-energy X-ray diffraction. Journal of Structural Biology 152, 14-27.

Almer, J.D., Stock, S.R., 2007. Micromechanical response of mineral and collagen phases in bone. Journal of Structural Biology 157, 365-370.

Barkaoui, A., Chamekh, A., Merzouki, T., Hambli, R., Mkaddem, A., 2014. Multiscale approach including microfibril scale to assess elastic constants of cortical bone based on

neural network computation and homogenization method. International Journal for Numerical Methods in Biomedical Engineering 30, 318-338.

Bini, F., Marinozzi, A., Marinozzi, F., Patanè, F., 2002. Microtensile measurements of single trabeculae stiffness in human femur. Journal of Biomechanics 35, 1515-1519.

Brennan, O., Kennedy, O.D., Lee, T.C., Rackard, S.M., O'Brien, F.J., 2009. Biomechanical properties across trabeculae from the proximal femur of normal and ovariectomised sheep. Journal of Biomechanics 42, 498-503.

Busse, B., Hahn, M., Soltau, M., Zustin, J., Püschel, K., Duda, G.N., Amling, M., 2009. Increased calcium content and inhomogeneity of mineralization render bone toughness in osteoporosis: mineralization, morphology and biomechanics of human single trabeculae. Bone 45, 1034-1043.

Carretta, R., Lorenzetti, S., Müller, R., 2013a. Towards patient-specific material

modeling of trabecular bone post-yield behavior. International Journal for Numerical Methods in Biomedical Engineering 29, 250-272.

Carretta, R., Stüssi, E., Müller, R., Lorenzetti, S., 2013b. Within subject heterogeneity in tissue-level post-yield mechanical and material properties in human trabecular bone. Journal of the Mechanical Behavior of Biomedical Materials 24, 64-73.

Carretta, R., Luisier, B., Bernoulli, D., Stüssi, E., Müller, R., Lorenzetti, S., 2013c. Novel method to analyze post-yield mechanical properties at trabecular bone tissue level. Journal of the Mechanical Behavior of Biomedical Materials 20, 6-18.

Choi, K., Goldstein, S,A., 1992. A comparison of the fatigue behavior of human trabecular and cortical bone tissue. Journal of Biomechanics 25, 1371-1381.

Dong, X.N., Almer, J.D., Wang, X., 2011. Post-yield nanomechanics of human cortical bone in compression using synchrotron X-ray scattering techniques. Journal of

Biomechanics 44, 676-682.

Feng, L., Jasiuk, I., 2011. Multi-scale characterization of swine femoral cortical bone. Journal of Biomechanics 44, 313-320.

Fujisaki, K., Tadano, S., Sasaki, N., 2006. A method on strain measurement of HAP in cortical bone from diffusive profile of X-ray diffraction. Journal of Biomechanics 39, 579-586.

Fujisaki, K., Tadano, S., 2007. Relationship between bone tissue strain and lattice strain of HAp crystals in bovine cortical bone under tensile loading. Journal of Biomechanics 40, 1832-1838.

Gibson, V.A., Stover, S.M., Gibeling, J.C., Hazelwood, S.J., Martin, R.B., 2006. Osteonal effects on elastic modulus and fatigue life in equine bone. Journal of Biomechanics 39, 217-225.

Giri, B., Almer, J.D., Dong, X.N., Wang, X., 2012. In situ mechanical behavior of mineral crystals in human cortical bone under compressive load using synchrotron X-ray scattering techniques. Journal of the Mechanical Behavior of Biomedical Materials 14, 101-112.

Giri, B., Tadano, S., Fujisaki, K., Sasaki, N., 2009. Deformation of mineral crystals in cortical bone depending on structural anisotropy. Bone 44, 1111-1120.

Gupta, H.S., Seto, J., Wagermaier, W., Zaslansky, P., Boesecke, P., Fratzl, P., 2006. Cooperative deformation of mineral and collagen in bone at the nanoscale. Proceedings of the National Academy of Sciences 103, 17741-17746.

Halgrin, J., Chaari, F., Markiewicz, É., 2012. On the effect of marrow in the mechanical behavior and crush response of trabecular bone. Journal of the Mechanical Behavior of Biomedical Materials 5, 231-237.

Hambli, R., Barkaoui, A., 2012, Physically based 3D finite element model of a single mineralized collagen microfibril. Journal of Theoretical Biology 301, 28-41.

Hambli, R., Thurner, P.J., 2013. Finite element prediction with experimental validation of damage distribution in single trabeculae during three-point bending tests. Journal of the Mechanical Behavior of Biomedical Materials 27, 94-106.

Hernandez, C.J., Tang, S.Y., Baumbach, B.M., Hwu, P.B., Sakkee, A.N., Van der Ham, F., DeGroot, J., Bank, R.A., Keaveny, T.M., 2005. Trabecular microfracture and the influence of pyridinium and non-enzymatic glycation-mediated collagen cross-links. Bone 37, 825-832.

Hoc, T., Henry, L., Verdier, M., Aubry, D., Sedel, L., Meunier, A., 2006. Effect of microstructure on the mechanical properties of Haversian cortical bone. Bone 38 466-474.

Jungmann, R., Szabo, M.E., Schitter, G., Tang, R.Y., Vashishth, D., Hansma, P.K., Thurner, P.J., 2011. Local strain and damage mapping in single trabeculae during three-point bending tests. Journal of the Mechanical Behavior of Biomedical Materials 4, 523-534.

Lievers, W.B., Waldman, S.D., Pilkey, A.K., 2010. Minimizing specimen length in elastic testing of end-constrained cancellous bone. Journal of the Mechanical Behavior of Biomedical Materials 3, 22-30.

Lorenzetti, S., Carretta, R., Müller, R., Stüssi, E., 2011. A new device and method for measuring the elastic modulus of single trabeculae. Medical Engineering & Physics 33, 993-1000.

Lucchinetti, E., Thomann, D., Danuser, G., 2000. Review Micromechanical testing of bone trabeculae - potentials and limitations. Journal of Materials Science 35,

6057-6064.

McNamara, L.M., Ederveen, A.G.H., Lyons, C.G., Price, C., Schaffler, M.B., Weinans, H., Prendergast, P.J., 2006. Strength of cancellous bone trabecular tissue from normal, ovariectomized and drug-treated rats over the course of ageing. Bone 39, 392-400.

Mittra, E., Rubin, C., Qin, Y.X., 2005. Interrelationship of trabecular mechanical and microstructural properties in sheep trabecular bone. Journal of Biomechanics 38, 1229-1237.

Perilli, E., Baleani, M., Öhman, C., Baruffaldi, F., Viceconti, M., 2007. Structural parameters and mechanical strength of cancellous bone in the femoral head in osteoarthritis do not depend on age. Bone 41, 760-768.

Rho, J.Y., Ashman, R.B., Turner, C.H., 1993. Young's modulus of trabecular and cortical bone material: ultrasonic and microtensile measurements. Journal of Biomechanics 26,

111-119.

Rho, J.Y., Roy 2nd, M.E., Tsui, T.Y., Pharr, G.M., 1999. Elastic properties of microstructural components of human bone tissue as measured by nanoindentation. Journal of Biomedical Materials Research 45, 48-54.

Rokita, E., Chevallier, P., Mutsaers, P.H.A., Tabor, Z., Wróbel, A., 2005. Studies of crystal orientation and calcium distribution in trabecular bone. Nuclear Instruments and Methods in Physics Research Section B 240, 69-74.

Smith, L.J., Schirer, J.P., Fazzalari, N.L., 2010. The role of mineral content in determining the micromechanical properties of discrete trabecular bone remodeling packets. Journal of Biomechanics 43, 3144-3149.

Stock, S.R., Yuan, F., Brinson, L.C., Almer, J.D., 2011. Internal strain gradients quantified in bone under load using high-energy X-ray scattering. Journal of

Biomechanics 44, 291-296.

Szabó, M.E., Taylor, M., Thurner, P.J., 2011. Mechanical properties of single bovine trabeculae are unaffected by strain rate. Journal of Biomechanics 44, 962-967.

Tadano, S., Giri, B., 2011. X-ray diffraction as a promising tool to characterize bone nanocomposites. Science and Technology of Advanced Materials 12, 064708.

Tadano, S., Giri, B., Sato, T., Fujisaki, K., Todoh, M., 2008. Estimating nanoscale deformation in bone by X-ray diffraction imaging method. Journal of Biomechanics 41, 945-952.

Tjhia, C.K., Odvina, C.V., Rao, D.S., Stover, S.M., Wang, X., Fyhrie, D.P., 2011. Mechanical property and tissue mineral density differences among severely suppressed bone turnover (SSBT) patients, osteoporotic patients, and normal subjects. Bone 49, 1279-1289.

Topoliński, T., Cichański, A., Mazurkiewicz, A., Nowicki, K., 2011. Study of the behavior of the trabecular bone under cyclic compression with stepwise increasing amplitude. Journal of the Mechanical Behavior of Biomedical Materials 4, 1755-1763.

Wolfram, U., Wilke, H.J., Zysset, P.K., 2010. Rehydration of vertebral trabecular bone: influences on its anisotropy, its stiffness and the indentation work with a view to age, gender and vertebral level. Bone 46, 348-354.

Yamada, S., Tadano, S., 2010. Residual stress around the cortical surface in bovine femoral diaphysis. Journal of Biomechanical Engineering 132, 044503.

Yamada, S., Tadano, S., Fujisaki, K., 2011a. Residual stress distribution in rabbit limb bones. Journal of Biomechanics 44, 1285-1290.

Yamada, S., Tadano, S., Todoh, M., Fujisaki, K., 2011b. Residual stress distribution in

the bovine femoral diaphysis measured by synchrotron. Journal of Biomechanical Science and Engineering 6, 114-124.

Yamada, S., Tadano, S., 2013. Effects of growth on residual stress distribution along the radial depth of cortical cylinders from bovine femurs. Journal of Biomechanics 46, 2130-2136.

Yamada, S., Tadano, S., Fujisaki, K., Kodaki, Y., 2013. Influence of osteon area fraction and degree of orientation of HAp crystals on mechanical properties in bovine femur. Journal of Biomechanics 46, 31-35.

Yamada, S., Tadano, S., Onuma, M., 2014. X-ray diffraction technique with imaging plate for detecting surface distribution of residual stress in diaphysis of bovine femurs. Experimental Mechanics 54, 633-640.

Figure and table legends

Figure 1 Specimen preparation and determination of trabecular orientation

(a) Trabeculae that were at least 3 mm in length were collected from the proximal epiphysis of three adult bovine femurs. The trabecular orientation α was defined as the angle between the trabecular axis and the bone axis. (b) The specimens were fixed onto thin metal jigs using superglue for tensile tests. Two small ink marks were placed on the surface of the ends of the specimens to serve as gauge points. (c) To determine the bone axis, which was defined as the longitudinal direction of the diaphysis, the part of diaphysis of the femurs was CT-scanned. The centroid point of the perimeter line of the diaphysis in each cross-section was obtained from the CT images, and the bone axis was calculated by approximating a straight line through those points.

Figure 2 The tensile testing device for a single trabecula

It consisted of a uniaxial stage and a load cell. The tissue strain was measured from the distance between the gauge points by microscopy.

Figure 3 Measurement setup for XRD experiments to obtain (a) the HAp crystal orientation and (b) the HAp crystal strain

Figure 4 Typical stress–strain relationships of a single trabecula under tensile loading

The tensile tests of each sample were conducted three times and the same color dots indicate the values in a test.

Figure 5 Typical XRD pattern of a single trabecula detected with X-ray IP

The X-rays diffracted from the (002) plane appeared as arcs in the upper and bottom parts of the IP image. The *c*-axis of HAp crystals was aligned with the trabecular axis.

Figure 6 (a) Relationship between E and $\langle\cos^2\beta\rangle$. (b) Typical relationship between HAp crystal strain ε^H and applied tissue strain ε in a single trabecula under tensile loading. The HAp crystal strain linearly increased with the applied tissue strain. The trend of the relation was calculated as the strain ratio $\varepsilon^H/\varepsilon$. (c) Relationship between E

and $\varepsilon^H/\varepsilon$. Strong positive correlations were observed in the trabeculae (r = 0.79; P < 0.001) and in all data, including the results of the cortical bone specimens (r = 0.86; P < 0.001). (d) Relationship between E and v_{Ca+P}. The values of E, $\varepsilon^H/\varepsilon$, and $\langle\cos^2\beta\rangle$ of the cortical bone in the bone axis were taken from the results of a previous study (Yamada et al., 2013).

Table 1 The number of samples examined in each experiment after excluding the unavailable data: μ-CT scan, tensile test, X-ray diffraction (XRD) measurements, and energy dispersive X-ray spectrometry (EDS). The mean values and standard deviations of each parameter are indicated: trabecular orientation (α), average cross-sectional area (A), circularity (Cir), aspect ratio (AR), elastic modulus (E), degree of c-axis orientation of the crystals with respect to the trabecular axis ($\langle\cos^2\beta\rangle$), strain ratio ($\varepsilon^H/\varepsilon$), and weight content of calcium and phosphorus (v_{Ca+P}). [*]In three specimens, the intensity of diffracted X-rays was too low for analysis. [†]A specimen was broken before the experiment. Furthermore, although the other two specimens were broken during the experiments, $\varepsilon^H/\varepsilon$ was calculated from the available data before rupture.

Figures and Tables

Figure 1

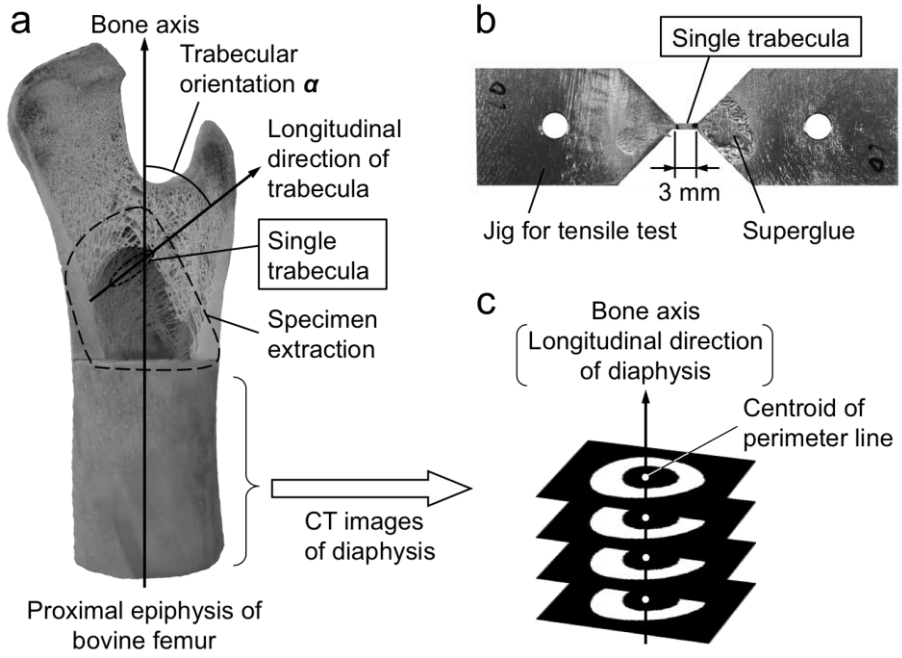

Figure 2

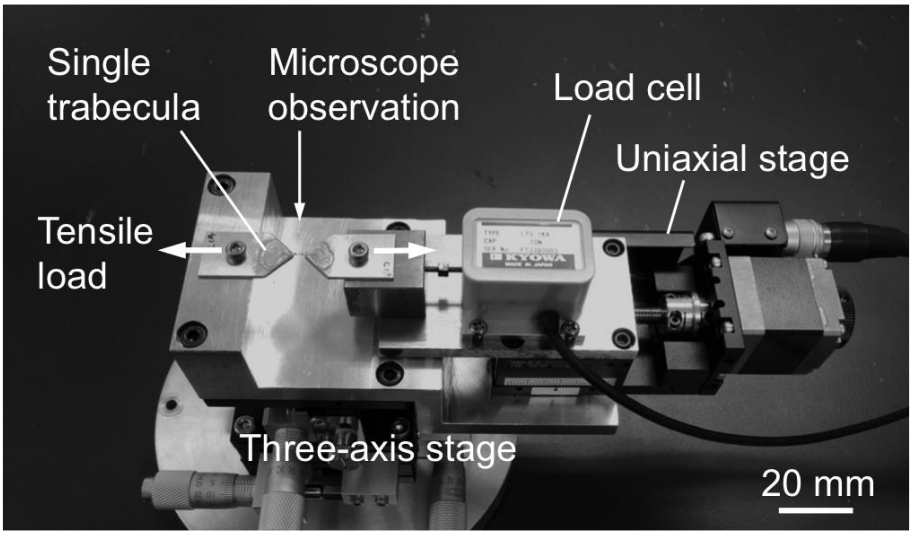
Single trabecula
Microscope observation
Load cell
Uniaxial stage
Tensile load
Three-axis stage
20 mm

Figure 3

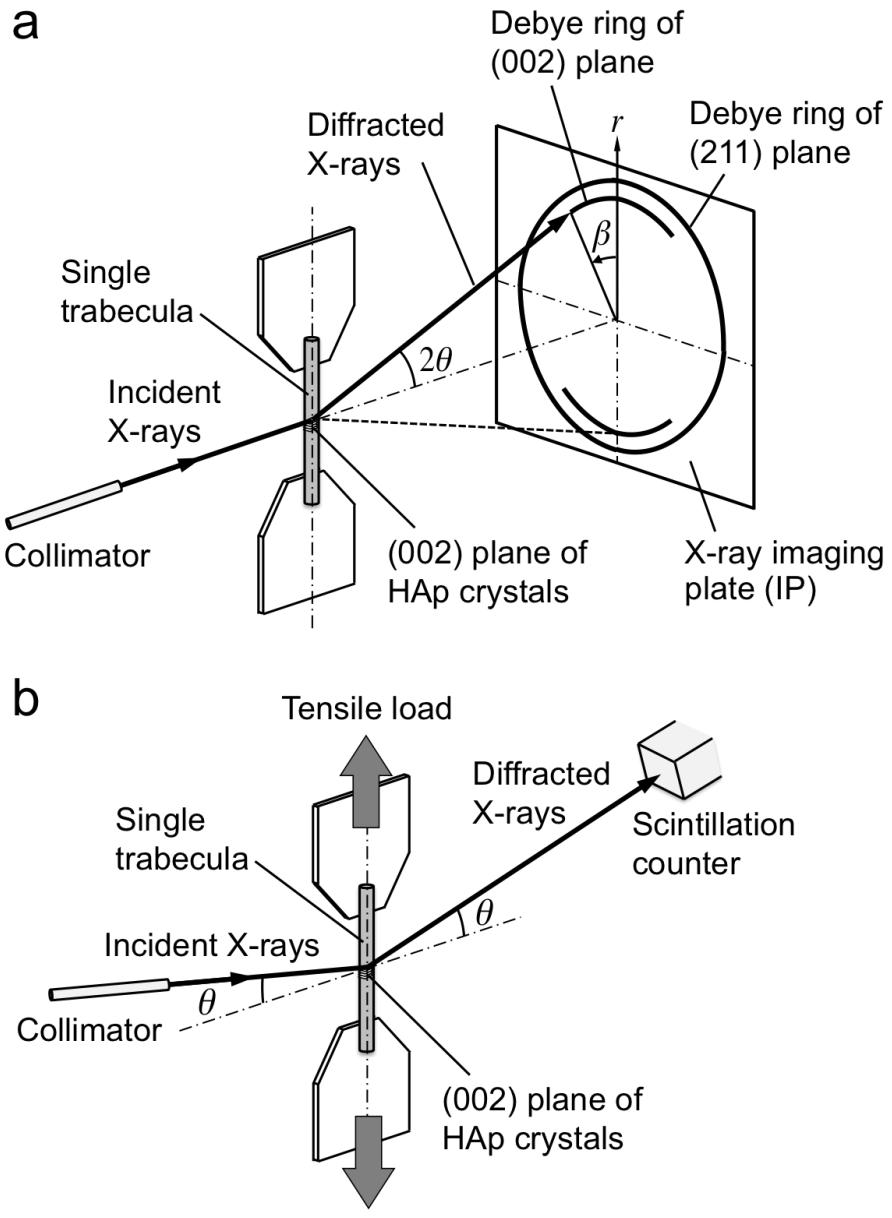
a
Debye ring of
(002) plane
Debye ring of
(211) plane
Diffracted
X-rays
r
β
Single
trabecula
2θ
Incident
X-rays
Collimator
(002) plane of
HAp crystals
X-ray imaging
plate (IP)
b
Tensile load
Diffracted
X-rays
Scintillation
counter
Single
trabecula
θ
Incident X-rays
θ
Collimator
(002) plane of
HAp crystals

Figure 4

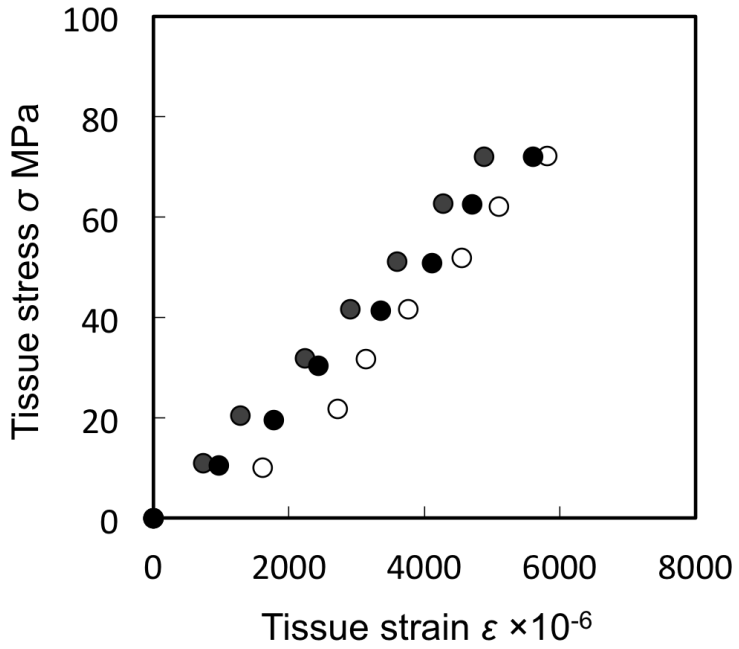
100
80
60
40
20
0
Tissue stress σ MPa
0
2000
4000
6000
8000
Tissue strain ε ×10-6

Figure 5

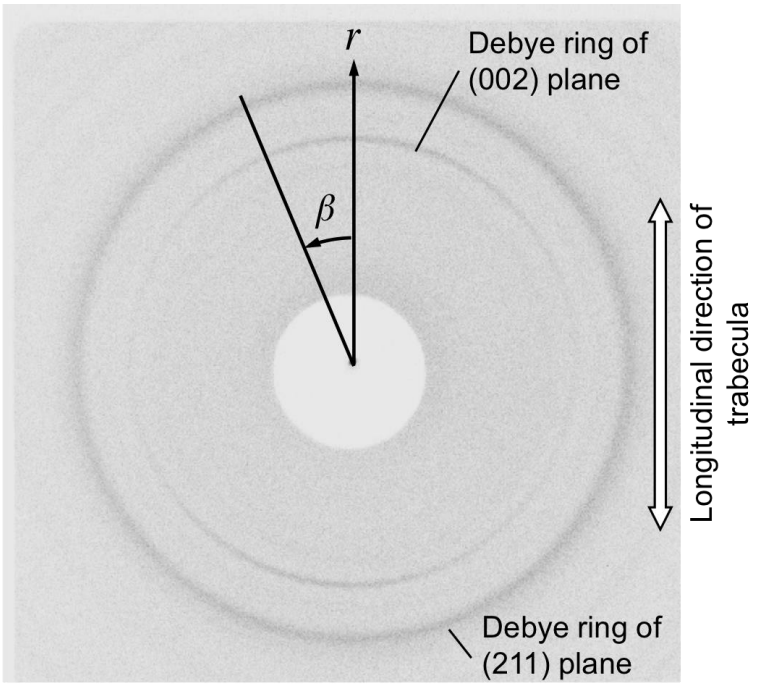
r
Debye ring of
(002) plane
β
Longitudinal direction of
trabecula
Debye ring of
(211) plane

Figure 6

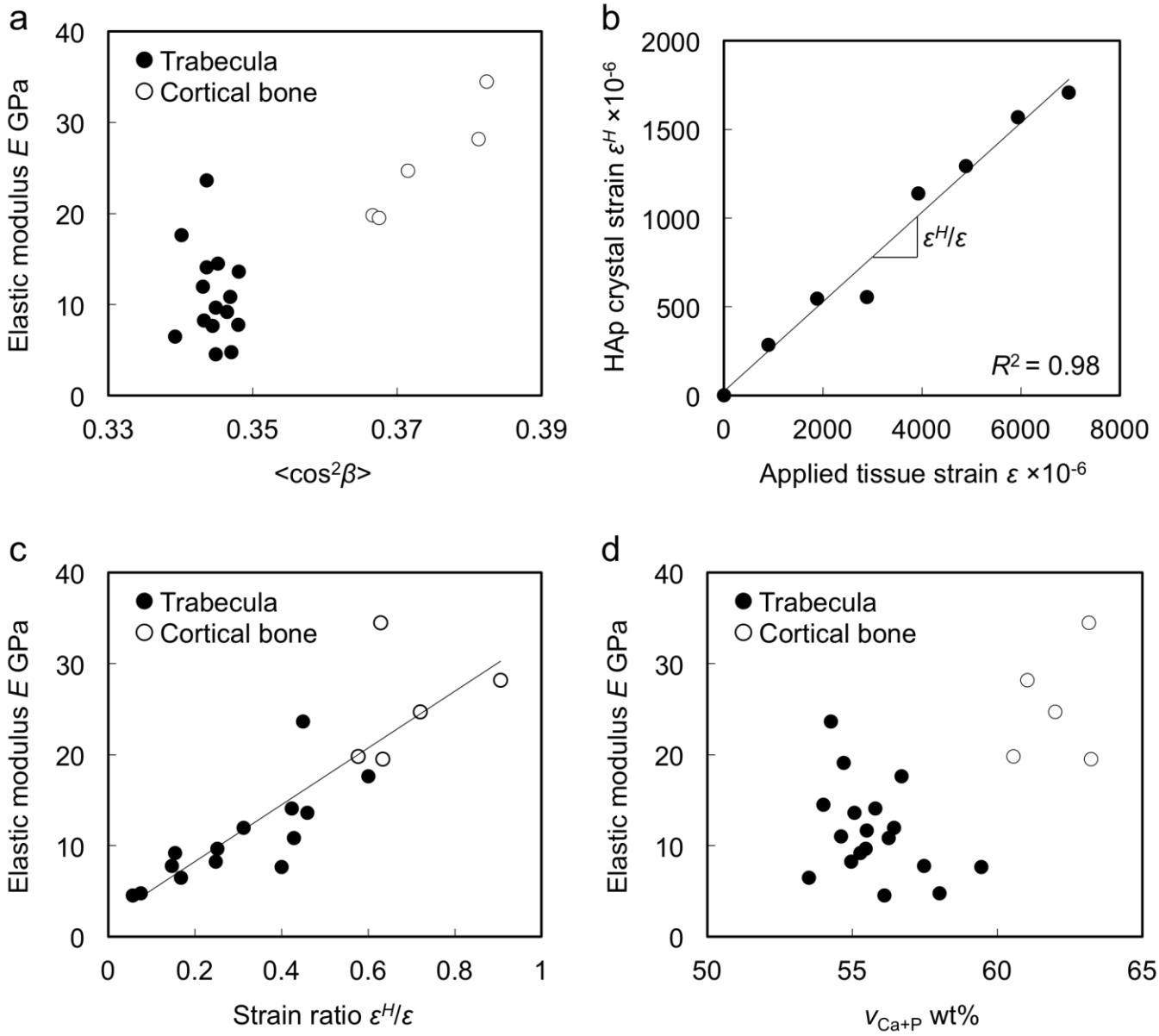
a
Elastic modulus E GPa
Trabecula
Cortical bone
<cos²β>
b
HAp crystal strain ε^H ×10^-6
ε^H/ε
R² = 0.98
Applied tissue strain ε ×10^-6
c
Elastic modulus E GPa
Trabecula
Cortical bone
Strain ratio ε^H/ε
d
Elastic modulus E GPa
Trabecula
Cortical bone
v_Ca+P wt%

Table 1

Experiments	μ-CT				Tensile test	XRD		EDS
Parameters	α (°)	A (mm^2)	*Cir*	*AR*	E (GPa)	$\langle\cos^2\beta\rangle$	$\varepsilon^H/\varepsilon$	v_{Ca+P}
No. specimens	18	18	18	18	18	15[*]	14[*, †]	18
Mean	53.6	0.152	0.825	1.58	11.5	0.345	0.298	55.8
s.d.	24.7	0.085	0.066	0.33	5.0	0.003	0.166	1.5